University of Dundee

Pharmacological validation of N-myristoyltransferase as a drug target in Leishmania donovani

Corpas Lopez, Victoriano; Moniz, Sonia; Thomas, Michael; Wall, Richard; Torrie, Leah; Zander-Dinse, Dorothea; Tinti, Michele; Brand, Stephen; Stojanovski, Laste; Manthri, Sujatha; Hallyburton, Irene; Zuccotto, Fabio; Wyatt, Paul; De Rycker, Manu; Horn, David; Ferguson, Michael; Clos, Joachim; Read, Kevin; Fairlamb, Alan; Gilbert, Ian; Wyllie, Susan

Link to publication in Discovery Research Portal

Pharmacological Validation of *N*-Myristoyltransferase as a Drug Target in *Leishmania donovani*

Victoriano Corpas-Lopez,[†,⊥] Sonia Moniz,[†,⊥] Michael Thomas,[†,⊥] Richard J. Wall,[†] Leah S. Torrie,[†] Dorothea Zander-Dinse,[‡] Michele Tinti,[†] Stephen Brand,[†,∥] Laste Stojanovski,[†] Sujatha Manthri,[†] Irene Hallyburton,[†] Fabio Zuccotto,[†] Paul G. Wyatt,[†] Manu De Rycker,[†] David Horn,[†] Michael A. J. Ferguson,[†] Joachim Clos,[‡] Kevin D. Read,[†] Alan H. Fairlamb,[†] Ian H. Gilbert,*[†] and Susan Wyllie*[†]

†The Wellcome Trust Centre for Anti-Infectives Research, School of Life Sciences, University of Dundee, Dow Street, Dundee DD1 5EH, United Kingdom

‡Leishmaniasis Group, Bernhard Nocht Institute for Tropical Medicine, Hamburg D-20359, Germany

S Supporting Information

ABSTRACT: Visceral leishmaniasis (VL), caused by the protozoan parasites *Leishmania donovani* and *L. infantum*, is responsible for ∼30 000 deaths annually. Available treatments are inadequate, and there is a pressing need for new therapeutics. *N*-Myristoyltransferase (NMT) remains one of the few genetically validated drug targets in these parasites. Here, we sought to pharmacologically validate this enzyme in *Leishmania*. A focused set of 1600 pyrazolyl sulfonamide compounds was screened against *L. major* NMT in a robust high-throughput biochemical assay. Several potent inhibitors were identified with marginal selectivity over the human enzyme. There was little correlation between the enzyme potency of these inhibitors and their cellular activity against *L. donovani* axenic amastigotes, and this discrepancy could be due to poor cellular uptake due to the basicity of these compounds. Thus, a series of analogues were synthesized with less basic centers. Although most of these compounds continued to suffer from relatively poor antileishmanial activity, our most potent inhibitor of *Lm*NMT (DDD100097, K_i of 0.34 nM) showed modest activity against *L. donovani* intracellular amastigotes (EC$_{50}$ of 2.4 μM) and maintained a modest therapeutic window over the human enzyme. Two unbiased approaches, namely, screening against our cosmid-based overexpression library and thermal proteome profiling (TPP), confirm that DDD100097 (compound **2**) acts on-target within parasites. Oral dosing with compound **2** resulted in a 52% reduction in parasite burden in our mouse model of VL. Thus, NMT is now a pharmacologically validated target in *Leishmania*. The challenge in finding drug candidates remains to identify alternative strategies to address the drop-off in activity between enzyme inhibition and *in vitro* activity while maintaining sufficient selectivity over the human enzyme, both issues that continue to plague studies in this area.

KEYWORDS: *Leishmania, N-myristoyltransferase, thermal proteome profiling (TPP), drug discovery, target validation*
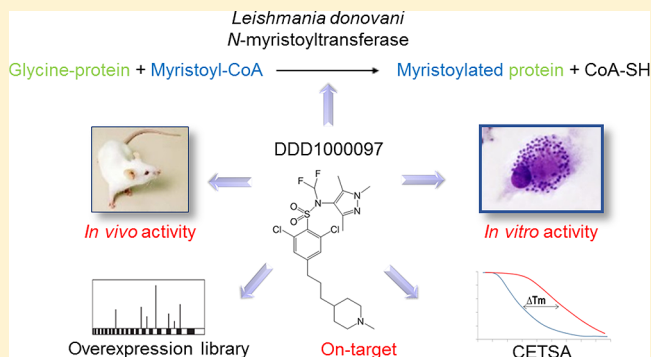
Visceral leishmaniasis (VL), caused by infection with the protozoan parasites *Leishmania donovani* and *L. infantum*, is the second largest parasitic killer after malaria with more than 200 million people currently at risk from infection. In 95% of cases, death can be prevented by timely and appropriate drug therapy.[1] However, current treatment options are far from ideal with the best available therapies for VL being miltefosine and liposomal amphotericin B (AmBisome).[2] Both drugs are superior to previous therapies such as pentavalent antimonials,[3] but they also have limitations. The principal drawbacks of miltefosine are its teratogenicity, prolonged treatment regimen, and high resistance potential.[4] Problems associated with amphotericin B include high treatment costs, an intravenous route of administration, requirement for a cold chain, and unresponsiveness in some Sudanese VL patients.[5] Thus, there remains a definite and urgent need to strengthen the range of treatment options for VL. Unfortunately, there are currently no new therapeutics in clinical development and relatively few in preclinical development[2,6,7] (https://www.dndi.org/diseases-projects/leishmaniasis/leish-portfolio/). Drug discovery efforts have been hampered by a paucity of well-validated molecular drug targets in *Leishmania*, with the molecular targets of the current clinically used drugs unknown. As a result, drug discovery programs for VL have become

heavily reliant upon whole cell (phenotypic) screening, despite such screens suffering from extremely low hit rates.[8]

N-Myristoyltransferase (NMT, EC 2.3.1.97) remains one of the very few robustly validated drug targets in the Kinetoplastida. The enzyme catalyzes the co- and post-translational addition of myristic acid (C14:0) onto the *N*-terminal glycine of specific proteins.[9,10] *N*-Myristoylation is believed to play a crucial role in the correct cellular localization and biological function of such modified proteins. NMT has been extensively studied in a number of organisms including humans, *Trypanosoma brucei*, *T. cruzi*, and *Leishmania spp*.[9,11−15] In these parasites, NMT has been demonstrated as essential for viability either by classical gene knockout with episomal rescue or by RNA interference, indicating that the *N*-myristoylation of certain proteins is an essential biological process. However, despite the development of numerous high affinity inhibitors capable of inhibiting the recombinant enzyme in assays and selectively targeting NMT in cells,[14−18] this enzyme has only been pharmacologically validated in the African trypanosome, where DDD85646, a low nM inhibitor of the enzyme, was able to cure a mouse model of stage one African sleeping sickness.[11] While it is tempting to assume that NMT will be equally amenable to pharmacological intervention in disease models of VL and Chagas' disease, this is not certain to be the case. *T. brucei* is acutely sensitive to NMT inhibition, and this is largely attributed to the perturbation of endocytosis, which occurs at exceptionally high rates in bloodstream trypanosomes.[19] Rates of endocytosis are likely to be considerably slower in *Leishmania*[20] and *T. cruzi*,[21] raising the possibility that these parasites may be less susceptible to inhibition of this biological process. Several previous studies have reported that potent, tight binding inhibitors of the *L. major* and *T. cruzi* NMT enzymes do not translate as potent inhibitors of their respective parasites *in vitro*.[14,22] In the most comprehensive of these studies,[22] Wright and colleagues confirm that two tight binding inhibitors are capable of inhibiting *N*-myristoylation in *L. donovani*, providing the first direct evidence of on-target engagement with NMT in this parasite. Indeed, this study demonstrates that the degree of engagement of these inhibitors with NMT in *Leishmania* parasites correlates directly with levels of cell killing.

Here, we describe the development of potent and selective *L. donovani* NMT inhibitors. We use two unbiased methodologies to confirm on-target activity in cells and, for the first time, demonstrate efficacy of our lead compound in a mouse model of VL. The implications of these findings for the development of more potent and efficacious NMT inhibitors for the treatment of VL are discussed.

■ RESULTS AND DISCUSSION

Discovery. Previously, we reported a pyrazolyl sulfonamide series that emerged from a high-throughput compound library screen against *Trypanosoma brucei N*-myristoyltransferase (*Tb*NMT) (Figure 1, exemplified by compound **1**).[11] As a result of these studies, a number of potent NMT inhibitors were developed including the lead compound DDD85646 which was curative in mouse models of stage 1 Human African Trypanosomiasis (HAT). Unfortunately, this compound was not active against the stage 2 HAT mouse model, where parasites infect the central nervous system (CNS). This treatment failure was attributed to poor penetration of the blood−brain barrier, thus preventing therapeutic levels of DDD85646 reaching the brain. To combat these issues, a
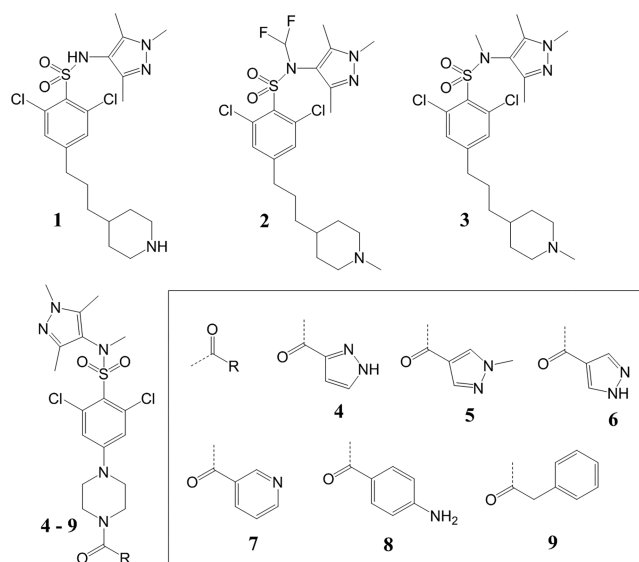

Figure 1. Chemical structures.

number of pyrazolyl sulfonamide analogues were developed with the strategy of reducing polar surface area and capping the sulphonamide to improve CNS penetration. This led to the discovery of DDD100097 (Figure 1, compound **2**) which was a potent inhibitor of *Tb*NMT and demonstrated moderate efficacy in the stage 2 mouse model.[23]

Compound **2** and other compounds synthesized in this medicinal chemistry program were collated to form a focused set of 1600 compounds selected for screening against *L. major* NMT in a biochemical enzymatic assay. The format of this 384-well assay was broadly similar to that previously described for *Tb*NMT,[11] with the same biotinylated CAP5.5 peptide used as a substrate. Key aspects of the assay development are summarized in Figure 2. The optimal enzyme concentration, assay linearity with respect to time, and Michaelis constants for CAP5.5 and myristoyl CoA were determined. The K_m^{app} for myristoyl CoA was determined to be 21 ± 4 nM and 1.0 ± 0.1 μM for CAP5.5 (Figure 2B,C). This assay returned a robust Z' value of 0.7 ± 0.05 ($n = 112$) and successfully identified a number of potent *Lm*NMT inhibitors, with 130 compounds inhibiting enzyme activity by >90% at 1 μM, a hit rate of 8.1%. However, a counter-screen of these compounds against human NMT revealed a pronounced lack of selectivity in most cases, with a comparison of potencies demonstrating a strong correlation (Figure 3A). The most potent inhibitors of *Lm*NMT were the methylpiperidine analogues **2** (*N*-difluoromethylsulfonamide) and **3** (methylsulfonamide) with pIC$_{50}$ values of 9.0 and 8.8, respectively (Figure 1 and Table 1), and demonstrating ~10-fold selectivity over the human enzyme. The most promising *Lm*NMT inhibitors were then screened against *L. donovani* axenic amastigotes (extracellular, mammalian stage). Unfortunately, there was little correlation between enzyme inhibition and antileishmanial activity, with drop-offs in activity of up to 1000-fold commonly observed (Figure 3B). Similar results have been reported elsewhere,[17,22] where this lack of translation was linked to both weak target engagement and poor cellular uptake due to the presence of a basic nitrogen that would be charged at physiological pH, thus reducing cellular permeability.

In order to identify potential strategies to overcome this issue, we interrogated a previously reported crystallographic
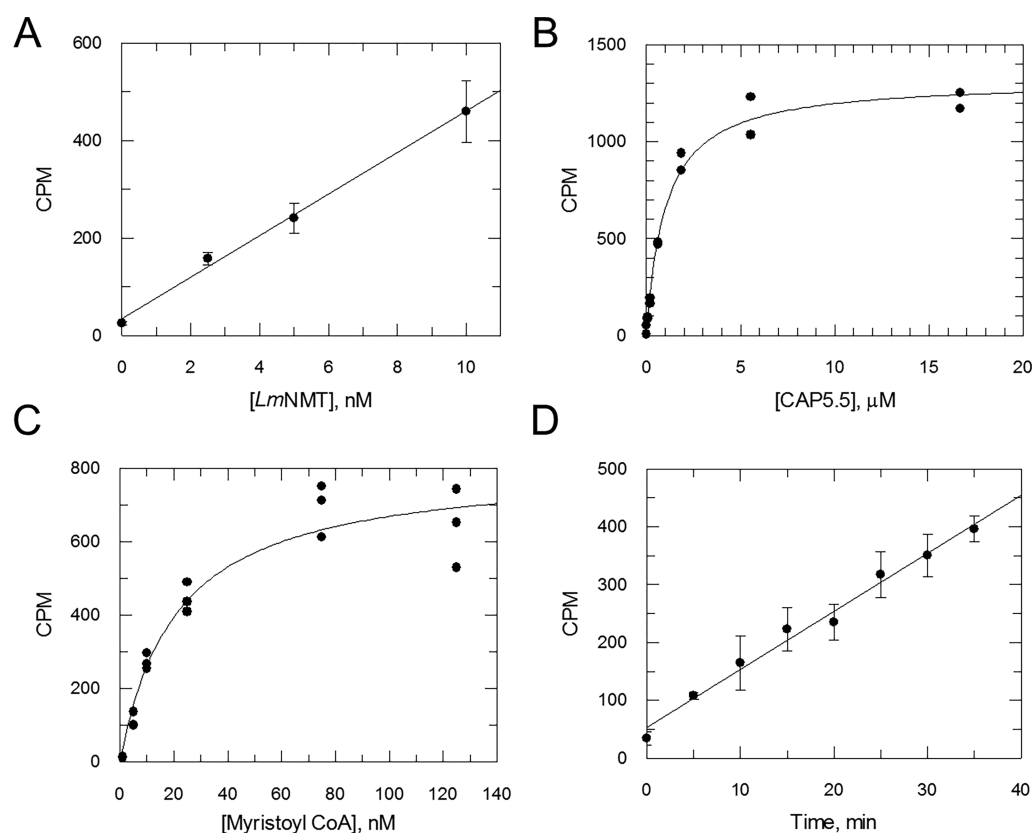
Figure 2. *Lm*NMT assay development. (A) Linearity of the assay with respect to enzyme concentration (data shown as mean CPM ± SD, $n = 3$). (B) CAP5.5 K_m determination (all data points shown, $n = 2$). (C) Myristoyl CoA K_m determination (all data points shown, $n = 3$). (D) Assay linearity with respect to time under the final assay conditions of 5 nM *Lm*NMT, 0.5 μM CAP5.5, and 125 nM myristoyl CoA (data shown as mean CPM ± SD, $n = 3$).
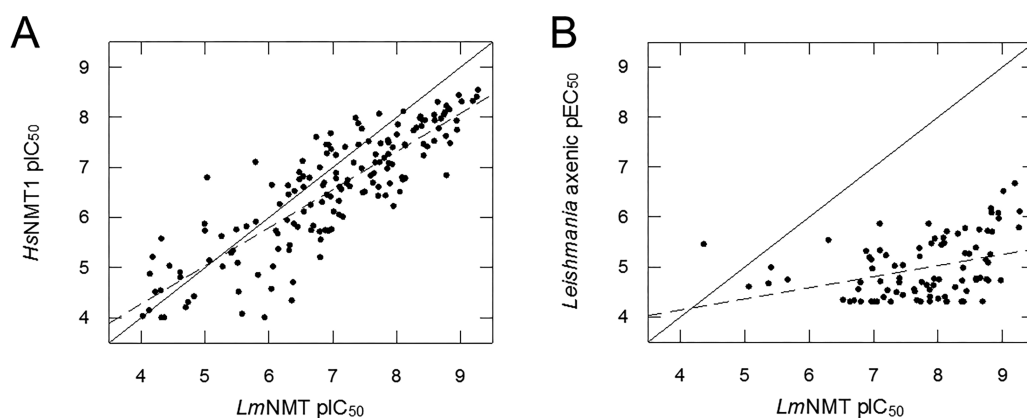

Figure 3. Enzymatic and cellular efficacy of *Ld*NMT inhibitors. (A) Correlation of pIC_{50} values for a focused set of compounds against *Lm*NMT and *Hs*NMT1 in enzymatic assays. Solid line represents equipotent activity while the dashed line represents a linear regression of the data ($r^2 = 0.856$). (B) Correlation of potencies for a focused set of compounds against *Lm*NMT (pIC_{50}) in enzymatic assays versus *L. donovani* axenic amastigotes (pEC_{50}) cell-based assays. Solid line represents equipotent activity while the dashed line represents a linear regression of the data ($r^2 = 0.358$).

structure of *Lm*NMT with compound **1** bound in the active site.[23] The structure highlighted the water-mediated interaction of the piperidine nitrogen with the catalytic α-carboxylate of the terminal leucine as being crucial for potency, in agreement with previous studies.[24] Therefore, a series of analogues were designed and synthesized where the basic piperidine was replaced with various heterocycles capable of making this key interaction, but with a much less basic center (Figure 1, compounds **4–9**). Several of these analogues, where

the piperidine was replaced by pyrazoles (compounds **4–6**), a pyridine (compound **7**), or an aniline (compound **8**), retained potency against *Lm*NMT in the submicromolar range (Figure 1, Table 1). The poor activity of compound **9**, where the piperidine was replaced with a phenyl group incapable of forming these key hydrogen bonds, again substantiated the importance of the targeted carboxylate interaction.

Screening of this cohort of compounds against axenic amastigotes again revealed a significant drop-off in enzyme

Table 1. Enzyme Inhibition and Cellular Data for NMT Inhibitors

compound ID	abbreviation	LmNMT IC$_{50}$, μM	HsNMT IC$_{50}$, μM	promastigote EC$_{50}$, μM	axenic amastigote EC$_{50}$, μM	intramacrophage EC$_{50}$, μM	THP-1 EC$_{50}$, μM	pK_a[c]
DDD99758	1	0.4	0.1	>50	>50	>50	>50	basic
DDD100097	2	0.0010[a]	0.01	0.04 ± 0.001	0.2 ± 0.006	2.4 ± 0.8	15.8	basic
DDD90146	3	0.0016[b]	0.02	0.07 ± 0.004	8.2 ± 0.6	7.1 ± 1.1	>50	basic
DDD101161	4	0.03	0.02	18.3 ± 0.1	2.7 ± 0.08	>50	>50	weakly acidic
DDD101163	5	0.08	0.08	10.0 ± 0.4	9.2 ± 0.4	>50	>50	neutral
DDD101172	6	0.06	0.1	>50	>50	>50	>50	neutral
DDD101173	7	0.1	0.5	5.8 ± 0.4	0.3 ± 0.01	>50	>50	weakly basic
DDD101177	8	0.03	0.008	8.2 ± 0.5	5.1 ± 0.2	>50	>50	neutral
DDD101169	9	10.0	6.3	6.3 ± 0.3	2.2 ± 0.03	40.5 ± 13.4	>50	neutral

[a]Estimated K_i value is 0.34 nM for this tight-binding inhibitor (see Materials and Methods). [b]Estimated K_i value is 0.38 nM for this tight-binding inhibitor (see Materials and Methods). [c]pK_a values were calculated for each compound using the Jaguar pK_a prediction component in the Schrodinger Small molecule platform (Supplementary Table 1 and Supplementary Figure 1).
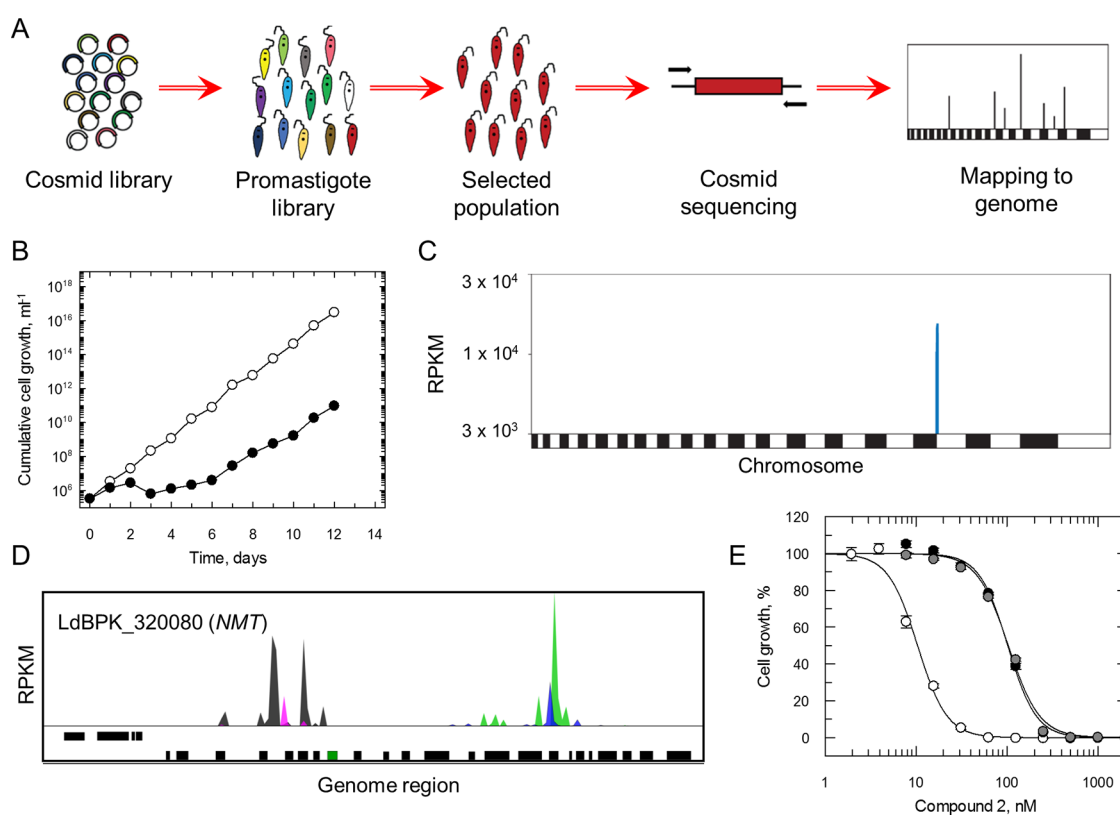

Figure 4. Target deconvolution utilizing a cosmid library approach. (A) Schematic representing the cosmid library workflow. (B) Cumulative growth of cosmid library population treated with compound **2** (80 nM, closed circles) and untreated (open circles). (C) Genome-wide map indicating cosmid library hits from screening of compound **2**. A single primary hit was identified, indicated in blue. (D) Focus on primary "hit" on chromosome 32. NMT (LdBPK_320080), green bar; other genes, black bars. The blue/pink and black/green peaks indicate independent cosmid inserts in different orientations. (E) Dose response curves of compound **2** against promastigotes constitutively overexpressing NMT (clone 1, black circles; clone 2, gray circles) and WT promastigotes (open circles). Data are the mean ± SD of three technical replicates and are representative of two independent experiments.

versus cellular potency (50−430-fold), with the only exception being the 3-pyridyl analogue (compound **7**), where enzymatic and antileishmanial activities were relatively similar (Table 1). This characteristic drop-off in activity was even more pronounced when compounds were screened against our *L. donovani* intracellular amastigote assay.[25] Indeed, only three of the nine compounds tested demonstrated any activity against these intracellular parasites at the concentrations tested, with compound **2** being the most potent (EC$_{50}$ value of 2.4 ± 0.8 μM). Interestingly, compound **2** also demonstrates

moderate activity against the intracellular amastigote form of the related Kinetoplastid parasite *T. cruzi* (EC$_{50}$ value of 0.47 μM compared with 5.1 μM against host Vero cells). Of particular note, compound **7** returned an EC$_{50}$ value of >50 μM despite showing submicromolar activity against axenic amastigotes suggesting that the lack of translation between enzyme and cellular potency is not driven solely by the effect of the basic nitrogen on cellular permeability potency.

On-Target Activity. The lack of correlation between our enzyme and cell-based data could potentially be explained by
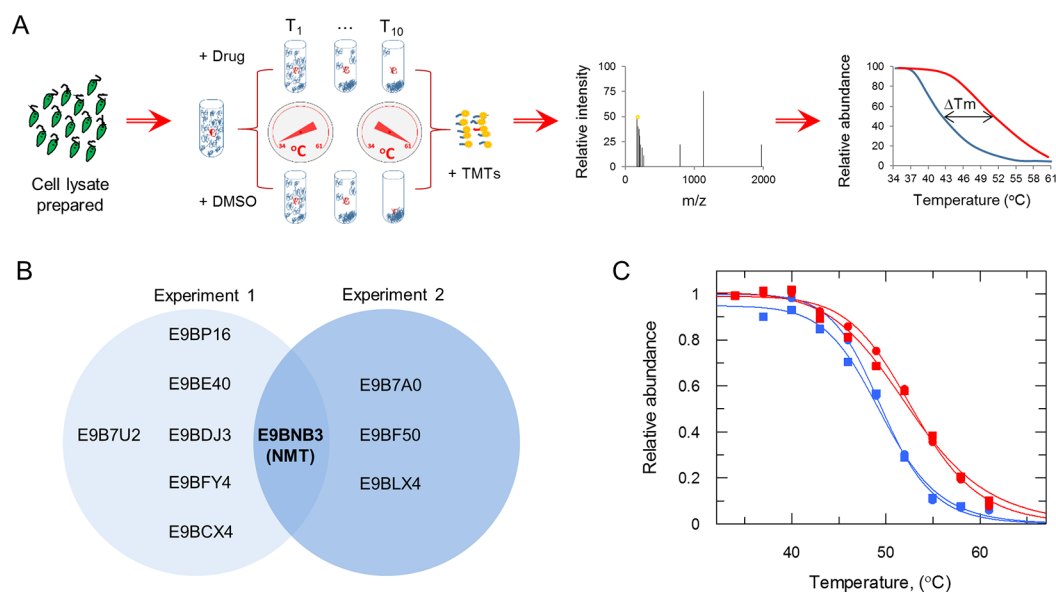
Figure 5. Target deconvolution utilizing TPP. (A) Schematic representing our TPP workflow. TMT: tandem mass tags. (B) Venn diagram of proteins identified as candidate targets of compound **2** from duplicate experiments (biological replicates). UniProt identifiers are used to represent individual proteins. (C) Melting curves for *L. donovani* NMT following incubation with 0.4 μM compound **2** (red) or vehicle (0.1% DMSO, blue). Data from two technical replicates (circles and squares) are shown, and the mean shift in melting temperature (ΔT_m) for NMT was 3.3 °C. Data from an independent duplicate experiment is presented in Supplementary Figure 2 and Supplementary Table 4.

compounds drifting off-target within parasites. To address this possibility, we used two unbiased approaches to identify the specific molecular target(s) of our most promising compound (compound **2**) in *L. donovani* promastigotes. In the first instance, we screened this compound against our genome-wide cosmid-based overexpression library (Figure 4). The principle behind this approach is that overexpression of a drug target can result in resistance to the corresponding drug by increasing the pool of functional protein or by reducing free drug through binding. The workflow for library construction and screening is illustrated in Figure 4A. This high-coverage library was constructed using a pcosTL cosmid backbone containing fragments of Sau3AI partially digested genomic DNA (35−45 kb). The pooled cosmids were then transfected into promastigotes. Prior to compound screening, cosmids harbored by the transfected parasites were harvested and analyzed by next generation sequencing. pcosTL-derived "barcodes" were used to precisely map overexpressed fragments to the reference *Leishmania* genome (LdBPK282A1). This analysis confirmed that our transfected library provided a genome coverage of >15-fold and also that 99% of genes were represented in the library.

Compound **2** was screened against the transfected library at a concentration equivalent to 2× EC$_{50}$ value (80 nM) (Figure 4B) until the growth of treated parasites was equivalent to that of the untreated (12 days). Cosmids maintained by the "resistant" population were harvested, sequenced and enriched fragments were mapped to the *L. donovani* genome. This screen revealed a single major hit on chromosome 32 comprising >44% of all mapped reads (Figure 4C, Supplementary Table 2). No other notable hits were identified from this screen. Closer inspection of this 50-kb region revealed 18 barcode pairs indicating that a mixed population of cosmid fragments overlapping this area of the genome was enriched by selection with this compound (Figure 4D). All enriched cosmid fragments contained LdBPK_320080, the gene encoding *Ld*NMT, providing strong evidence that this enzyme

is the target of compound **2**. Of the other genes in this region, only LdBPK_320090.1 possessed a putative myristoylation signal. This putative signal is also present in the orthologues of other *Leishmania* species but absent in the *T. brucei* and *T. cruzi* orthologues. Moreover, the possibility of LdBPK_320090.1 conferring resistance by outcompeting compound **2** in the active site of NMT seems unlikely, particularly as this protein does not appear to be myristoylated in whole cells.[22] Finally, we confirmed that overexpression of NMT in *L. donovani* promastigotes results in an ∼10-fold decrease in sensitivity to this pyrazolyl sulphonamide (Figure 4E).

Thermal proteome profiling (TPP) was used as an additional approach to confirm on-target engagement of compound **2**. TPP is based on the principle that binding of a drug to its protein target can significantly increase the thermal stability of that protein.[26] The workflow for our TPP strategy is illustrated in Figure 5A. Briefly, clarified lysates of *L. donovani* promastigotes were incubated in the presence of compound **2** (10× established EC$_{50}$ value) or DMSO vehicle. Aliquots of lysate (drug and vehicle treated) were then incubated at designated temperatures (between 34 and 61 °C), and for each temperature, insoluble (denatured) proteins were removed. The resulting soluble protein samples were reduced, alkylated, and digested with trypsin prior to derivatization with tandem mass tags (TMT). Pooled peptides were fractionated by HPLC and analyzed by LC/MS-MS prior to identification and quantitation. The melting points of identified proteins were then established using the TPP software package.

Two independent TPP experiments, each comprised of two technical replicates, were carried out with compound **2** (0.4 μM). The top 25 proteins demonstrating thermal shift in the presence of this compound from experiments 1 and 2 are shown in Supplementary Tables 3 and 4. Of these, 7 proteins from experiment 1 and 4 proteins from experiment 2 were classified as legitimate "hits" or target candidates by the TPP software package which applies strict selection criteria based on

data quality (see Materials and Methods for details). The only target candidate common to both data sets was *Ld*NMT (Figure 5B). Individual melting curves revealed that the thermal stability of *Ld*NMT increased by 3.3 °C (ΔT_m) in experiment 1 and 4.8 °C in experiment 2 (Figure 5C and Supplementary Figure 2). It should be noted that TPP studies provide evidence of on-target engagement rather than direct evidence of inhibition of *N*-myristoylation. Nonetheless, these findings support the results of our cosmid-based over-expression library and the shift in potency observed with our NMT-overexpressing cell line in confirming *Ld*NMT as the molecular target of compound **2**.

***In Vivo* Efficacy of Compound 2.** Despite a growing number of studies describing medicinal chemistry strategies to target *Leishmania* NMT,[16,24,27−29] to the best of our knowledge, none of the resulting compounds have been reported as active *in vivo*. Thus, NMT remains to be pharmacologically validated in *Leishmania spp*. This stage of drug target validation is often overlooked but is one the most robust since it addresses several key issues:[30,31] first, whether a particular mode of action can have the required pharmaco-logical response in an *in vivo* setting and, second, whether the particular compound series has suitable pharmacokinetic properties to address the target. Specifically, these studies confirm that a given target can be sufficiently inhibited by dosing of drug-like small molecules to elicit parasite death, in the absence of host toxicity. With this in mind, compound **2** was selected for assessment in our mouse model of VL.[6] The selection of this compound for a proof-of-concept efficacy study was principally based not only on its promising potency in intramacrophage assays but also on its previously demonstrated oral bioavailability in mice.[23] Oral dosing with compound **2** at 50 mg kg^{-1} b.i.d. over 5 days resulted in a 52% reduction in parasite burden (Figure 6), compared to vehicle dosed control animals. This level of efficacy is identical to that seen with sodium stibogluconate sodium stibogluconate (52% reduction), albeit with an increased dose and increased dosing frequency, although some way short of the reduction of parasite burden achieved with miltefosine (88% reduction). Collectively, these data demonstrate NMT as a pharmacolog-ically validated drug target in *Leishmania* for the first time.

CONCLUSIONS

Target-based approaches to drug discovery for parasitic diseases have proved problematic and are often plagued by poor translation of enzyme activity to cellular potency and ultimately *in vivo* efficacy. NMT remains one of the very few robustly validated drug targets in the kinetoplastids having been confirmed as genetically essential for the survival of *T. brucei*, *T. cruzi*, and *Leishmania spp*. While potent inhibitors of NMT in *T. brucei* have proved effective in treating animal models of stage 1 and 2 sleeping sickness, similarly potent inhibitors developed against the *Leishmania* enzyme suffer from considerable drop-offs in activity against both axenic and intracellular amastigotes. In this study, our strategy was to reduce the basicity of inhibitors active against *Lm*NMT with the rationale that this was likely to improve cell permeability. Unfortunately, this approach was not successful in improving cellular potency, raising the possibility that this precipitous drop in activity may be due to other factors. One possible explanation is that *Leishmania* are simply less susceptible to inhibition of NMT than other organisms. Alternatively, using compounds similar to those described in our current study,
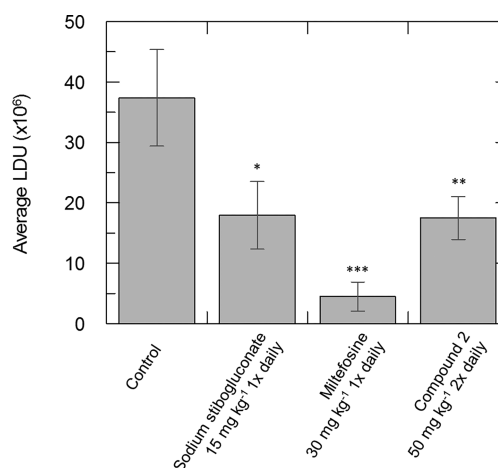

Figure 6. Efficacy of compound **2** in a mouse model of VL. Efficacy of compound **2** was assessed at 50 mg kg^{-1} b.i.d. for 5 days, alongside vehicle (orally administered b.i.d. for 5 days), miltefosine (orally administered 30 mg kg^{-1} q.d. for 5 days), and sodium stibogluconate (administered by subcutaneous injection at 15 mg kg^{-1} q.d. for 5 days). Each arm was carried out with 5 mice. Mean reduction in parasite burden expressed as Leishman Donovan Units (LDU), equivalent to the number of amastigotes per 500 nucleated cells multiplied by the organ weight in milligrams. Treatment with miltefosine resulted in an 88% reduction in liver parasite burden, while dosing with both compound **2** and sodium stibogluconate resulted in 52% reductions. Unpaired *t* tests confirmed the reduction in parasitaemia evident in all three groups of treated mice is significant, compared to untreated control animals, with $P = 0.0021$ (*), $P < 0.0001$ (***), and $P = 0.0009$ (**) for sodium stibogluconate, miltefosine, and compound **2**, respectively.

Wright and colleagues provided quantitative evidence that the degree of inhibitor engagement with NMT in *Leishmania* parasites correlates directly with cell killing, suggesting that the drop-off in activity for this series may simply be due to weak engagement with the target in the cell.[22] We were able to confirm that our most promising compound acts on-target in *L. donovani* using two unbiased orthogonal approaches and that targeting of NMT can considerably reduce parasite burden *in vivo*. Confirmation of NMT as a pharmacologically validated target in *Leishmania* is significant. This study provides realistic hope that future NMT inhibitors may prove curative in a VL mouse model and have potential in a clinical setting. The challenge remains to identify strategies to address the drop-off in activity between enzyme inhibition and *in vitro* activity while maintaining sufficient selectivity over the human enzyme. Understanding the principal reasons for this drop-off in activity will be crucial in informing our future chemical strategy: whether this is due to permeability issues due to the charge of the molecule or if significantly more potent compounds are required due to the lower susceptibility of *Leishmania* to inhibition of NMT.

MATERIALS AND METHODS

General Chemistry. Chemicals and solvents were purchased from Sigma-Aldrich, Alfa Aesar, Apollo Scientific, Fluorochem, and TCI UK and were used as received. Air and moisture sensitive reactions were carried out under an inert atmosphere of nitrogen. Analytical thin-layer chromatography (TLC) was performed using precoated TLC plates (layer of 0.20 mm silica gel 60 with fluorescent indicator UV254, from Merck). Developed plates were air-dried and analyzed under a

UV lamp (UV254/365 nm) and/or with chemical stains where appropriate. Flash column chromatography was performed using prepacked silica gel cartridges (230−400 mesh, 35−70 μm, from Teledyne ISCO) using a Teledyne ISCO CombiFlash Rf. ^{1}H NMR were recorded on a Bruker Avance DPX 500 spectrometer (at 500.1 MHz), a Bruker Avance III HD (at 400.1 MHz), or a Bruker Avance DPX 300 (at 299.9 MHz). Chemical shifts (δ) are expressed in ppm recorded using the residual solvent as the internal reference in all cases. Signal splitting patterns are described as singlet (s), doublet (d), triplet (t), quartet (q), multiplet (m), broad (br), or a combination thereof. LC-MS analyses were performed with either an Agilent HPLC 1100 series connected to a Bruker Daltonics MicrOTOF or an Agilent Technologies 1200 series HPLC connected to an Agilent Technologies 6130 quadrupole LC/MS, where both instruments were connected to an Agilent diode array detector and all final compounds were >95% purity. LCMS chromatographic separations were conducted with either a Waters XBridge C18 column, 50 mm × 2.1 mm, 3.5 μm particle size, or Waters XSelect C18 column, 30 mm × 2.1 mm, 2.5 μm particle size; mobile phase was water/acetonitrile + 0.1% HCOOH or water/acetonitrile + 0.1% NH₃. Preparative HPLC separations were performed with a Waters mass-directed HPLC (system fluidics organizer, 2545 binary gradient module, 2 × 515 HPLC pumps, 2767 sample manager) connected in parallel to a Waters 3100 mass detector and a 2998 photodiode array detector.

4 - 9
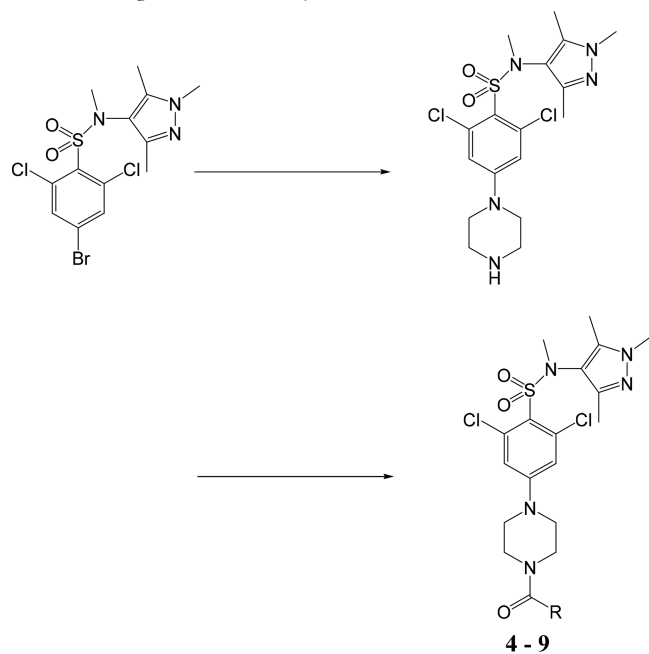
2,6-Dichloro-N-methyl-4-(piperazin-1-yl)-N-(1,3,5-tri-methyl-1H-pyrazol-4-yl)benzenesulfonamide. A mixture of 4-bromo-2,6-dichloro-N-methyl-N-(1,3,5-trimethyl-1H-pyr-azol-4-yl)benzenesulfonamide[23] (2.12 g, 5 mmol), cesium carbonate (3.26 g, 10 mmol), xantphos (288 mg, 0.5 mmol), and tris(dibenzylideneacetone)dipalladium(0) (228 mg, 0.25 mmol) in 1,4-dioxane (25 mL) was degassed and stirred at 65 °C overnight. After cooling, water (100 mL) and DCM (100 mL) were added and the organic layer was separated, evaporated, and purified by flash chromatography (10−100% EtOAc/heptane) to give the Boc-protected intermediate. This was taken up in DCM (5 mL)/TFA (5 mL) and stirred for 2 h. Solvent was evaporated, and crude material was dissolved in

methanol, loaded onto an SCX column, and eluted with 2 M NH₃/MeOH. Solvent was evaporated to give product which was used without further purification (590 mg, 1.37 mmol, 27%). ^{1}H NMR (CDCl₃): δ 6.80 (s, 2H), 3.69 (s, 3H), 3.38 (s, 3H), 3.30−3.26 (m, 4H), 3.03−2.98 (m, 4H), 2.15 (s, 3H), 1.87 (s, 3H).

4-(4-(1H-Pyrazole-5-carbonyl)piperazin-1-yl)-2,6-di-chloro-N-methyl-N-(1,3,5-trimethyl-1H-pyrazol-4-yl)-benzenesulfonamide (Compound 4). A solution of 2,6-dichloro-N-methyl-4-(piperazin-1-yl)-N-(1,3,5-trimethyl-1H-pyrazol-4-yl)benzenesulfonamide (80 mg, 0.19 mmol), TBTU (77 mg, 0.25 mmol), and DIPEA (75 μL, 4.4 mmol) was stirred for 5 min; 1H-pyrazole-5-carboxylic acid (25 mg, 0.23 mmol) was added and stirred for 4 h. The crude solution was purified directly by mass-directed HPLC to give 4 (35 mg, 0.067 mmol, 35%). ^{1}H NMR (CDCl₃): δ 7.65 (d, J = 2.4 Hz, 1H), 6.82 (m, 3H), 4.23−3.96 (m, 4H), 3.69 (s, 3H), 3.53−3.41 (m, 4H), 3.39 (s, 3H), 2.15 (s, 3H), 1.86 (s, 3H). MS (ESI): m/z 526.2, 528.2 [M + H]⁺.

2,6-Dichloro-N-methyl-4-(4-(1-methyl-1H-pyrazole-4-carbonyl)piperazin-1-yl)-N-(1,3,5-trimethyl-1H-pyrazol-4-yl)benzenesulfonamide (Compound 5). Compound 5 was synthesized by an analogous method to 4 using 1-methyl-1H-pyrazole-4-carboxylic acid (28 mg, 0.23 mmol) to give 23 mg (0.042 mmol, 22% yield). ^{1}H NMR (CDCl₃): δ 7.77 (s, 1H), 7.66−7.65 (m, 1H), 6.81 (s, 2H), 3.96 (s, 3H), 3.91−3.88 (m, 4H), 3.68 (s, 3H), 3.44−3.40 (m, 4H), 3.39 (s, 3H), 2.16 (s, 3H), 1.86 (s, 3H). MS (ESI): 540.2, 542.2 [M + H]⁺.

4-(4-(1H-Pyrazole-4-carbonyl)piperazin-1-yl)-2,6-di-chloro-N-methyl-N-(1,3,5-trimethyl-1H-pyrazol-4-yl)-benzenesulfonamide (Compound 6). Compound 6 was synthesized by an analogous method to 4 using 1H-pyrazole-4-carboxylic acid (25 mg, 0.23 mmol) to give 29 mg (0.055 mmol, 29% yield). ^{1}H NMR (CDCl₃): δ 7.90 (s, 2H), 6.81 (s, 2H), 3.94−3.89 (m, 4H), 3.69 (s, 3H), 3.45−3.40 (m, 4H), 3.39 (s, 3H), 2.15 (s, 3H), 1.86 (s, 3H). MS (ESI): m/z 526.2, 528.2 [M + H]⁺.

2,6-Dichloro-N-methyl-4-(4-nicotinoylpiperazin-1-yl)-N-(1,3,5-trimethyl-1H-pyrazol-4-yl)benzenesulfonamide (Compound 7). Compound 7 was synthesized by an analogous method to 4 using nicotinic acid (27 mg, 0.23 mmol) to give 22 mg (0.041 mmol, 22% yield). ^{1}H NMR (CDCl₃): δ 8.75−8.73 (m, 2H), 7.84−7.81 (m, 1H), 7.45−7.41 (m, 1H), 6.83 (s, 2H), 3.99−3.77 (m, 4H), 3.69 (s, 3H), 3.47−3.33 (m, 7H), 2.17 (s, 3H), 1.85 (s, 3H). MS (ESI): m/z 537.2, 539.2 [M + H]⁺.

4-(4-(4-Aminobenzoyl)piperazin-1-yl)-2,6-dichloro-N-methyl-N-(1,3,5-trimethyl-1H-pyrazol-4-yl)-benzenesulfonamide (Compound 8). Compound 8 was synthesized by an analogous method to 4 using 4-amino-benzoic acid (31 mg, 0.23 mmol) to give 30 mg (0.054 mmol, 28% yield). ^{1}H NMR (DMSO): δ 7.18 (d, J = 8.6 Hz, 2H), 7.04 (s, 2H), 6.57 (d, J = 8.6 Hz, 2H), 5.56 (bs, 2H), 3.62−3.57 (m, 7H), 3.47−3.43 (m, 4H), 3.25 (s, 3H), 1.96 (s, 3H), 1.79 (s, 3H). MS (ESI): m/z 551.2. 553.2 [M + H]⁺.

2,6-Dichloro-N-methyl-4-(4-(2-phenylacetyl)-piperazin-1-yl)-N-(1,3,5-trimethyl-1H-pyrazol-4-yl)-benzenesulfonamide (Compound 9). Compound 9 was synthesized by an analogous method to 4 using phenylacetic acid (30 mg, 0.23 mmol) to give 33 mg (0.060 mmol, 32% yield). ^{1}H NMR (CDCl₃): δ 7.39−7.27 (m, 5H), 6.75 (s, 2H), 3.83−3.79 (m, 4H), 3.69 (s, 3H), 3.63−3.59 (m, 2H), 3.38 (s,

3H), 3.34−3.30 (m, 2H), 3.15−3.11 (m, 2H), 2.16 (s, 3H), 1.85 (s, 3H). MS (ESI): m/z 550.2, 552.2 [M + H]$^+$.

Jaguar pK_a Predictions. pK_a values for the desired sites in compounds **1−9** were calculated by *ab initio* quantum mechanics using the Jaguar pK_a prediction component in the Schrodinger Small molecule platform (Schrödinger Release 2018-2: Jaguar, Schrödinger, LLC, New York, NY, 2018).[32] The Jaguar pK_a prediction module calculates the pK_a (or pK_b) of molecules that contain acidic or basic functional groups. The calculations involve geometry optimization of the ionic and neutral species and single-point energy and frequency calculations using the Self Consistent Field (SCF) method, plus an empirical correction. For each compound, a thorough conformational search was carried out and the 5 lowest energy conformers (within 12 kcal mol^{-1}) were used for pK_a calculation using water as solvent. Default parameters were used for SCF convergence. Different pseudospectral grid cut-offs were used for each compound, and results were averaged.

***Lm*NMT Recombinant Protein Expression and Purification.** Recombinant *Lm*NMT was expressed and purified as previously described.[33]

***Lm*NMT Enzymatic Assay.** *Lm*NMT assays were carried out at room temperature (22−23 °C) in 384-well white optiplates (PerkinElmer). Each assay was performed in a 40 μL reaction volume containing 30 mM Tris, pH 7.4, 0.5 mM EDTA, 0.5 mM EGTA, 1.25 mM dithiothreitol (DTT), 0.1% (v/v) Triton X-100, 0.125 μM [^{3}H]myristoyl-CoA (8 Ci mmol^{-1}) (PerkinElmer), 0.5 μM biotinylated CAP5.5 peptide substrate (GCGGSKVKPQPPQA[K-Biotin]) (Pepceuticals), 5 nM *Lm*NMT, and various concentrations of the test compound.

Test compound (0.4 μL in DMSO, final concentration of 1 μM) was transferred to all assay plates using a Cartesian Hummingbird (Genomics Solution) before 20 μL of enzyme was added to assay plates (with buffer only added to "no enzyme" control wells). The reaction was initiated with 20 μL of a substrate mix and stopped after 30 min with 40 μL of a stop solution containing 0.2 M phosphoric acid, pH 4.0, 1.5 M MgCl$_2$, and 1 mg mL^{-1} PVT SPA beads (GE Healthcare). All reaction mix additions were carried out using a Thermo Scientific WellMate (Matrix). Plates were sealed and read on a TopCount NXT Microplate Scintillation and Luminescence Counter (PerkinElmer).

ActivityBase from IDBS was used for data processing and analysis. All IC$_{50}$ curve fitting was undertaken using XLFit version 4.2 from IDBS. A four-parameter logistic dose−response curve was used using XLFit 4.2 Model 205. All test compound curves had floating top and bottom, and prefit was used for all four parameters.

K_i Calculations. K_i values were calculated for compounds **2** and **3**, identified as tight binding inhibitors in our enzyme inhibition assays.[34] The nominal concentration of NMT in these assays was 5 nM. Fitting the data to the IC$_{50}$ equation

$$\frac{v_i}{v_0} = \frac{1}{1 + \left(\frac{i}{IC_{50}}\right)^h}$$

(1)

yielded a value of 1.17 ± 0.07 nM for compound **2**, indicating that tight-binding inhibition was operative, since the lowest possible IC$_{50}$ value is half of the total active enzyme concentration (i.e., 2.5 nM).

Accordingly, these data were fitted to Morrison's quadratic equation for tight-binding inhibitors

$$\frac{v_i}{v_0} = 1 - \frac{([E]_T + [I]_T + K_i^{app}) - \sqrt{([E]_T + [I]_T + K_i^{app})^2 - 4[E]_T[I]_T}}{2[E]_T}$$

(2)

where v_i/v_0 is the fractional activity in the presence of inhibitor, E_T and I_T are the total concentrations of enzyme and inhibitor in the assay, and K_i^{app} is the apparent inhibition constant. This equation will fit all IC$_{50}$ data, provided the concentration of active enzyme is accurately known. Fitting by nonlinear regression with E_T as a variable returned an active enzyme concentration with a high error. Linear regression of the lowest inhibitor concentrations was used to obtain a more accurate estimate of the concentration of active enzyme. This yielded an estimate of 1.56 nM active NMT (correlation coefficient of 0.966). Using this value as a fixed parameter in the above equation yielded a K_i^{app} = 0.51 ± 0.08 nM (for compound **2**).

For a competitive inhibitor,

$$K_i^{app} = K_i\left(1 + \frac{[S]}{K_m}\right)$$

(3)

Substituting $[S]$ = 0.5 μM and K_m = 1.0 μM into the Cheng-Prusoff equation yields a K_i value of 0.34 nM for compound **2**. The K_i value of compound **3** was calculated in an identical manner.

Cell Lines and Culture Conditions. The clonal *L. donovani* cell line LdBOB (derived from MHOM/SD/62/1S-CL2D) was used in our *in vitro* compound screening and mechanism of action studies. Promastigotes were grown at 26 °C in modified M199 media with axenic amastigotes grown at 37 °C, as previously described.[35] All animal studies were carried using *L. donovani* (LV9; WHO designation: MHOM/ET/67/HU3).

***L. donovani* Intramacrophage, Axenic Amastigote, and Promastigote Compound Sensitivity Assays.** These assays were carried out as previously described.[25,36,37]

***In Vivo* Efficacy.** Groups of female BALB/c mice (5 per group) were inoculated intravenously with approximately 2 × 10^7 *L. donovani* amastigotes (LV9) harvested from the spleen of an infected hamster.[38] From day 7 postinfection, groups of mice were treated with drug vehicle only (orally), with miltefosine (30 mg kg^{-1} orally), with sodium stibogluconate (15 mg kg^{-1} subcutaneously), or with compound **2** (50 mg kg^{-1} orally). Miltefosine and sodium stibogluconate were dosed once daily for 5 days while compound **2** was dosed twice daily for 5 days. Dosing solutions were prepared fresh each day, and the vehicle used was Milli-Q H$_2$O (miltefosine and sodium stibogluconate) and 10% DMSO/60% PEG400/30% Milli-Q H$_2$O (compound **2**). On day 14 (5 days dosing groups), all animals were humanely euthanized; liver smears were made, and parasite burdens were determined by counting the number of amastigotes/500 liver cells.[37] Parasite burden is

expressed in Leishman Donovan Units (LDU): mean number of amastigotes per 500 liver cells × mg weight of liver.[39]

Ethical Statement. All regulated procedures, at the University of Dundee, on living animals were carried out under the authority of a project license issued by the Home Office under the Animals (Scientific Procedures) Act 1986, as amended in 2012 (and in compliance with EU Directive EU/2010/63). License applications are approved by the University's Ethical Review Committee (ERC) before submission to the Home Office. The ERC has a general remit to develop and oversee policy on all aspects of the use of animals on University premises and is a subcommittee of the University Court, its highest governing body.

Cosmid Library Generation. The cosmid backbone pcosTL[40] was a kind gift from John Kelly (London School of Hygiene and Tropical Medicine). The library was constructed essentially as described previously.[41] Briefly, pcosTL was digested sequentially with *Sma*I and *Bam*HI. The digested cosmid was then ligated with size-selected Sau3AI partial digest products of *L. donovani* (strain 1SR) genomic DNA. After packaging, using the Gigapack Gold II kit (Stratagene), the complexity of the library was tested and the library was amplified and stored at −70 °C. Mid-log *L. donovani* promastigotes (4×10^7 cells per transfection) were transfected with 10 µg of cosmid library DNA. Promastigotes maintaining cosmids were selected by the addition of G418 (125 µg mL^{-1}) to the culture medium. Parasites recovered from 36 transfections were pooled to build the final cosmid library. In total, 90 000 integrated genomic DNA fragments were recovered from our *Leishmania* library suggesting a final genome coverage of ∼15-fold.

Cosmid Library Screening. Cosmid-containing *L. donovani* promastigotes were maintained at a minimum concentration of 1×10^5 cells mL^{-1} (1.5×10^7 cells in total). Test compounds were added to the library at an initial concentration equivalent to 2× their established EC$_{50}$ values. Cell densities were monitored daily, and the library was subcultured before reaching 1×10^7 mL^{-1}, with addition of fresh test compound. In cases where the addition of test compounds (2× EC$_{50}$) had no impact on cell growth, higher concentrations were added. Libraries were continuously cultured in the presence of test compounds until there was a marked increase in cell growth suggesting the emergence of a selected, resistant promastigote population. Genomic DNA and accompanying cosmids were isolated from selected *L. donovani* promastigotes (1.5×10^9 cells in total) using a standard alkaline lysis protocol. The resulting DNA was transformed into ElectroMAX DH5α-E cells, and the resultant transformants (containing cosmids) were purified using a NucleoBond Xtra Midi Plus kit (Machery-Nagel).

Sequencing of Selected Cosmids. Purified cosmid DNA was sequenced using an Illumina HiSeq platform (Beijing Genomics Institute). Sequence reads were aligned to the *L. donovani* BPK282A1 genome sequence (v9.0, tritrypdb.org) using Bowtie2 software[42] with the following conditions: very-sensitive-local. The aligned files were then manipulated using SAMtools[43] and a custom python script[44] to identify reads with barcodes (CTCTTAAAAGCATCATGTCT and AGACATGATGCTTTTAAGAG). Reads were then quantified using the Artemis genome browser[45] and Excel.

Generation of *L. donovani* Cell Line Overexpressing *Ld*NMT. The NMT gene was amplified from *L. donovani* (LdBOB) genomic DNA using primers LdNMTbglIIFW (GATC<u>AGATCT</u>ATGTCTCGCAATCCATCGAACT) and LdNMTbglIIRV (GATC<u>AGATCT</u>CTACAACATCACC-AAGGCAACC) with gene-specific sequences flanked by BgIII sites (underlined). This resulting amplified fragment was digested with *Bgl*II prior to ligation into the similarly digested pIR1-SAT vector (a kind gift from Professor Steve Beverley). The validity of the construct was confirmed by sequencing. The resulting construct was digested with SwaI and transfected into *L. donovani* promastigotes. Transfected parasites were selected and maintained by selection with nourseothricin (100 µg mL^{-1}).

Quantitative RT-PCR. RNA was harvested from mid-log *L. donovani* promastigotes (1×10^8) using the RNeasy Mini Kit (Qiagen) and used to synthesize cDNA using an RNA-to-cDNA kit (Applied Biosystems), as per the manufacturers' instructions. Quantitative RT-PCR reactions were performed using Brilliant III Ultra-Fast QPCR Master Mix (Agilent Technologies) with the following cycling conditions: 95 °C for 3 min (1 cycle), 95 °C for 20 s, and 60 °C for 20 s (40 cycles). Relative quantification was established using the reference gene, rRNA45.[46] The level of NMT in the overexpression cell lines was normalized to wildtype using the $\Delta\Delta C_t$ method. Two independently transfected clones were used, and significance was measured using a student's unpaired *t* test.

***L. donovani* Lysate Preparation.** *L. donovani* (LdBOB) promastigotes were grown in large scale roller bottle cultures starting at an initial concentration of 1×10^5 cells mL^{-1} (1.5×10^7 cells in total). Cell were grown for 72 h, as previously described. Promastigotes were harvested by centrifugation (1912*g*, 15 min, 4 °C) and washed with ice-cold PBS (1912*g*, 5 min, 4 °C), and finally, the cell pellet was resuspended in 8 mL of ice-cold lysis buffer (1 mM EDTA, 1 mM DTT, 100 µM TLCK, and 1× Roche EDTA-free cOmplete protease inhibitor cocktail in 50 mM potassium phosphate buffer, pH 7.4). The cell suspension was submitted to 3 freeze−thaw cycles in a dry ice/ethanol bath to biologically inactivate the parasites and then submitted to cell disruption (Constant Systems, UK) at 30 kpsi. The resulting lysate was centrifuged (100 000*g*, 20 min, 4 °C); supernatant was collected, and the protein concentration was determined using the Bio-Rad Protein Assay.

Thermal Shift Assays. The lysate concentration was adjusted to 2.5 mg mL^{-1} with lysis buffer, and then, 2 × 2 mL aliquots were incubated at room temperature for 30 min in the presence of test compound (equivalent to 10× EC$_{50}$) or vehicle (0.1% DMSO). Each 2 mL aliquot (drug and vehicle treated) was divided into 10 × 100 µL aliquots in 0.5 mL thin-walled PCR tubes and incubated at a designated temperature (34, 37, 40, 43, 46, 49, 52, 55, 58, or 61 °C) for 3 min followed by incubation at RT for 3 min before each sample was placed on ice. Each aliquot was centrifuged (100 000*g*, 20 min, 4 °C); supernatants were collected, and the protein concentration was assessed.

Sample Processing. Samples were reduced by the addition of TCEP (25 mM final concentration) and incubated at 37 °C for 10 min. Alkylation was carried out by the addition of iodoacetamide (25 mM final concentration) and incubated at RT for 1 h in the dark. Samples were then digested by the addition of 1:50 LysC (Wako, Japan) in 100 mM triethylammonium bicarbonate (TEAB) followed by incubation at 37 °C for 6 h and then addition of 1:50 trypsin (Thermo) followed by incubation at 37 °C overnight. The efficiency of sample digestion efficiency was assessed by LC-

MS/MS (LTQ XL, Thermo). The samples were then vacuum-dried and resuspended in 100 mM TEAB (100 μL). Samples were then incubated in their respective tandem mass tag (TMT) 10-plex reagents (Thermo) for 1 h at RT with agitation. Reactions were quenched by the addition of 5% hydroxylamine for 15 min, and each set of samples (treated and vehicle) was pooled in the same tube and dried overnight. The TMT-labeled samples were dried and kept at −85 °C until further analysis.

Fractionation by HPLC. Pooled samples were resuspended in 200 μL of 10 mM ammonium formate (pH 9.5) and fractionated by high-pH reversed phase HPLC. A C18 column (XBridge peptide BEH, 130 Å, 3.5 μm, 2.1 × 150 mm, Waters) with a guard column (XBridge, C18, 3.5 μm, 2.1 × 10 mm, Waters) was used on an Ultimate 3000 HPLC (Thermo-Scientific). Ammonium formate (100 mM) was adjusted to pH 9.5 with ammonia and used to prepare buffer A (10 mM ammonium formate in Milli-Q water) and buffer B (10 mM ammonium formate, 90% acetonitrile). The column and guard column were equilibrated with 2% buffer B for 20 min at a constant flow rate of 0.2 mL min^{-1} for 20 min. Samples (180 μL) were loaded onto the column at 0.2 mL min^{-1}, and a separation gradient started 1 min after samples were loaded onto the column. Peptides were eluted from the column with a gradient of 2% buffer B to 20% B over 8 min then from 20% B to 47% B over 37 min. The column was then washed for 15 min with 100% buffer B. Fractions were collected from 1 to 80 min using a WPS-3000FC autosampler (Thermo-Scientific) at 1 min intervals. Fractions were pooled to give 20 pools of approximately equivalent peptide content (as judged by UV trace at 220 nm), dried in a Speedvac, and dissolved in 50 μL of 1% formic acid prior to analysis by LC-MS/MS.

LC-MS/MS. Analysis of peptides was performed on a Q-Exactive-HF (Thermo Scientific) mass spectrometer coupled to a Dionex Ultimate 3000 RS (Thermo Scientific). LC buffers used were as follows: buffer A (0.1% formic acid in Milli-Q water (v/v)) and buffer B (80% acetonitrile and 0.08% formic acid in Milli-Q water (v/v)). Aliquots of each sample (1 μL) were loaded at 5 μL·min^{-1} onto a trap column (100 μm × 2 cm, PepMap nanoViper C18 column, 5 μm, 100 Å, Thermo Scientific) equilibrated in 5% buffer B. The trap column was washed for 5 min at the same flow rate and then switched in-line with a Thermo Scientific resolving C18 column (75 μm × 50 cm, PepMap RSLC C18 column, 2 μm, 100 Å). Peptides were eluted from the column at a constant flow rate of 300 nL min^{-1} with a linear gradient from 5% buffer B (for pools 1−10) or 7% buffer B (for pools 11−20) to 35% buffer B over 130 min and then to 98% buffer B over 2 min. The column was then washed with 98% buffer B for 20 min and re-equilibrated in 5% buffer B for 17 min. The Q-exactive HF was used in data-dependent mode. A scan cycle comprised MS1 scan (m/z range from 335 to 1800, with a maximum ion injection time of 50 ms, a resolution of 120 000, and automatic gain control (AGC) value of 3 × 10^6) followed by 15 sequential dependent MS2 scans (with an isolation window set to 0.7 Da, resolution at 60 000, maximum ion injection time at 200 ms, and AGC of 1 × 10^5). To ensure mass accuracy, the mass spectrometer was calibrated immediately prior to analysis of the 20 fraction pools.

Peptide and Protein Identification and Quantitation. MS data were analyzed using the software MaxQuant (http://maxquant.org/, version 1.6.1.0). Carbamidomethyl (C), oxidation (M), acetyl (Protein N-term), deamidation (NQ),

and Gln→ pyro-Glu were set as variable-modifications. Proteins were identified by searching the MS and MS/MS data for the peptides against *L. donovani* strain BPK282A1 (UniProt Protein Knowledgebase). Trypsin/P and LysC/P were selected as the digestive enzyme with two potential missed cleavages. Reporter ion MS2 mode was selected using the TMT-10plex labels on N-termini and lysine epsilon-amino groups. Protein abundance was calculated according to the normalized reporter ion intensities. The FDR threshold for peptides and proteins was 0.01. FTMS MS/MS mass tolerance was set to 10 ppm, and ITMS MS/MS mass tolerance was 0.06 Da.

Thermal Proteome Profiling (TPP) Data Analysis. TPP experiments were analyzed using the TPP Package available in Bioconductor, as previously described.[47] Briefly, the MaxQuant protein group file was used to extract the raw protein abundance (reporter intensity corrected columns). Contaminant protein groups (e.g., non-*L. donovani* proteins), reverse sequence identifications, and "only identified by site hits" were removed from this list. TMT quantification was scaled by dividing each protein time point series by the intensity of the lowest temperature reporter (34 °C). The melting curves were calculated using a sigmoidal fitting approach with the R package TPP. This fitting was used to determine the melting point (T_m), which is defined as the temperature at which half of the amount of proteins was denatured. The melting point differences (ΔT_m) were calculated by subtracting the T_m values of treated and untreated samples. The sigmoidal melting curves were filtered according to the following criteria: melting curves must reach a relative abundance plateau of < 0.3, and the coefficient of determination (r^2) must be >0.8. The statistical significance was calculated by using the nonparametric analysis of response curves (NPARC) of the R package TPP. The significance threshold was set to $P < 0.05$. All proteomics data sets have been deposited with the PRoteomics IDEntifications (PRIDE) database.

■ ASSOCIATED CONTENT

Ⓢ Supporting Information

The Supporting Information is available free of charge on the ACS Publications website at DOI: 10.1021/acsinfecdis.8b00226.

Supplementary Table 1: calculated pK_a values; Supplementary Table 2: overexpression library "hits"; Supplementary Tables 3 and 4: top 25 proteins demonstrating thermal shift in the presence of compound **2** from experiments 1 and 2; Supplementary Figure 1: compound **3** in its lowest energy conformation used for pK_a calculation; Supplementary Figure 2: melting curves for *L. donovani* NMT following incubation with 0.4 μM compound **2** (experiment 2) (PDF)

■ AUTHOR INFORMATION

Corresponding Authors

*E-mail: s.wyllie@dundee.ac.uk.
*E-mail: i.h.gilbert@dundee.ac.uk.

ORCID Ⓞ

Michele Tinti: 0000-0002-0051-017X
Paul G. Wyatt: 0000-0002-0397-245X
Manu De Rycker: 0000-0002-3171-3519
Kevin D. Read: 0000-0002-8536-0130

Alan H. Fairlamb: 0000-0001-5134-0329
Ian H. Gilbert: 0000-0002-5238-1314
Susan Wyllie: 0000-0001-8810-5605

Present Address
‖S.B.: Medicines for Malaria Venture (MMV), PO Box 1826, 20 Route de Pré-Bois, 1215 Geneva 15, Switzerland.

Author Contributions
⊥V.C.-L., S.M., and M.T. contributed equally. Author contributions were as follows: V.C.-L., M.T., L.S.T., F.Z., M.D., and S.W. designed the research; V.C.-L., S.M., M.T., R.J.W., L.S.T., S.B., L.S., S.M., I.H. F.Z., and S.W. performed the research; M.T., L.S.T., M.D., F.Z., P.G.W., D.H., M.A.J.F., K.D.R., A.H.F, I.H.G., and S.W. supervised the research; J.C. and D.Z.-D. contributed new reagents; V.C-L, R.J.W., L.S.T, M.D., M.T., K.D.R, A.H.F., I.H.G., and S.W. analyzed data; M.T. and S.W. wrote the paper.

Notes
The authors declare no competing financial interest.

■ REFERENCES

(1) Ritmeijer, K., and Davidson, R. N. (2003) Médecins Sans Frontières interventions against kala-azar in the Sudan, 1989−2003. *Trans. R. Soc. Trop. Med. Hyg.* 97, 609−613.

(2) Nagle, A. S., Khare, S., Kumar, A. B., Supek, F., Buchynskyy, A., Mathison, C. J., Chennamaneni, N. K., Pendem, N., Buckner, F. S., Gelb, M. H., and Molteni, V. (2014) Recent developments in drug discovery for leishmaniasis and human African trypanosomiasis. *Chem. Rev.* 114 (22), 11305−11347.

(3) Ponte-Sucre, A., Gamarro, F., Dujardin, J. C., Barrett, M. P., Lopez-Velez, R., Garcia-Hernandez, R., Pountain, A. W., Mwenechanya, R., and Papadopoulou, B. (2017) Drug resistance and treatment failure in leishmaniasis: A 21st century challenge. *PLoS Neglected Trop. Dis.* 11 (12), e0006052.

(4) den Boer, M. L., Alvar, J., Davidson, R. N., Ritmeijer, K., and Balasegaram, M. (2009) Developments in the treatment of visceral leishmaniasis. *Expert Opin. Emerging Drugs* 14 (3), 395−410.

(5) Mueller, M., Ritmeijer, K., Balasegaram, M., Koummuki, Y., Santana, M. R., and Davidson, R. (2007) Unresponsiveness to AmBisome in some Sudanese patients with kala-azar. *Trans. R. Soc. Trop. Med. Hyg.* 101 (1), 19−24.

(6) Wyllie, S., Thomas, M., Patterson, S., Crouch, S., De Rycker, M., Lowe, R., Gresham, S., Urbaniak, M. D., Otto, T. D., Stojanovski, L., Simeons, F. R. C., Manthri, S., MacLean, L. M., Zuccotto, F., Homeyer, N., Pflaumer, H., Boesche, M., Sastry, L., Connolly, P., Albrecht, S., Berriman, M., Drewes, G., Gray, D. W., Ghidelli-Disse, S., Dixon, S., Fiandor, J. M., Wyatt, P. G., Ferguson, M. A. J., Fairlamb, A. H., Miles, T. J., Read, K. D., and Gilbert, I. H. (2018) Cyclin-dependent kinase 12 is a drug target for visceral leishmaniasis. *Nature* 560 (7717), 192−197.

(7) Khare, S., Nagle, A. S., Biggart, A., Lai, Y. H., Liang, F., Davis, L. C., Barnes, S. W., Mathison, C. J., Myburgh, E., Gao, M. Y., Gillespie, J. R., Liu, X., Tan, J. L., Stinson, M., Rivera, I. C., Ballard, J., Yeh, V., Groessl, T., Federe, G., Koh, H. X., Venable, J. D., Bursulaya, B., Shapiro, M., Mishra, P. K., Spraggon, G., Brock, A., Mottram, J. C.,

(8) Buckner, F. S., Rao, S. P., Wen, B. G., Walker, J. R., Tuntland, T., Molteni, V., Glynne, R. J., and Supek, F. (2016) Proteasome inhibition for treatment of leishmaniasis, Chagas disease and sleeping sickness. *Nature* 537 (7619), 229−233.

(8) Don, R., and Ioset, J. R. (2014) Screening strategies to identify new chemical diversity for drug development to treat kinetoplastid infections. *Parasitology* 141 (1), 140−146.

(9) Towler, D. A., Eubanks, S. R., Towery, D. S., Adams, S. P., and Glaser, L. (1987) Amino-terminal processing of proteins by N-myristoylation. Substrate specificity of N-myristoyl transferase. *J. Biol. Chem.* 262 (3), 1030−1036.

(10) Towler, D. A., Adams, S. P., Eubanks, S. R., Towery, D. S., Jackson-Machelski, E., Glaser, L., and Gordon, J. I. (1987) Purification and characterization of yeast myristoyl CoA:protein N-myristoyltransferase. *Proc. Natl. Acad. Sci. U. S. A.* 84 (9), 2708−2712.

(11) Frearson, J. A., Brand, S., McElroy, S. P., Cleghorn, L. A. T., Smid, O., Stojanovski, L., Price, H. P., Guther, M. L. S., Torrie, L. S., Robinson, D. A., Hallyburton, I., Mpamhanga, C. P., Brannigan, J. A., Wilkinson, A. J., Hodgkinson, M., Hui, R., Qiu, W., Raimi, O. G., van Aalten, D. M. F., Brenk, R., Gilbert, I. H., Read, K. D., Fairlamb, A. H., Ferguson, M. A. J., Smith, D. F., and Wyatt, P. G. (2010) N-myristoyltransferase inhibitors as new leads to treat sleeping sickness. *Nature* 464 (7289), 728−732.

(12) Price, H. P., Menon, M. R., Panethymitaki, C., Goulding, D., McKean, P. G., and Smith, D. F. (2003) Myristoyl-CoA: protein N-myristoyltransferase, an essential enzyme and potential drug target in kinetoplastid parasites. *J. Biol. Chem.* 278 (9), 7206−7214.

(13) Glover, C. J., Hartman, K. D., and Felsted, R. L. (1997) Human N-myristoyltransferase amino-terminal domain involved in targeting the enzyme to the ribosomal subcellular fraction. *J. Biol. Chem.* 272 (45), 28680−28689.

(14) Roberts, A. J., Torrie, L. S., Wyllie, S., and Fairlamb, A. H. (2014) Biochemical and genetic characterisation of *Trypanosoma cruzi* N-myristoyltransferase. *Biochem. J.* 459 (2), 323−332.

(15) Herrera, L. J., Brand, S., Santos, A., Nohara, L. L., Harrison, J., Norcross, N. R., Thompson, S., Smith, V., Lema, C., Varela-Ramirez, A., Gilbert, I. H., Almeida, I. C., and Maldonado, R. A. (2016) Validation of N-myristoyltransferase as potential chemotherapeutic target in mammal-dwelling stages of *Trypanosoma cruzi*. *PLoS Neglected Trop. Dis.* 10 (4), e0004540.

(16) Rackham, M. D., Yu, Z., Brannigan, J. A., Heal, W. P., Paape, D., Barker, K. V., Wilkinson, A. J., Smith, D. F., Leatherbarrow, R. J., and Tate, E. W. (2015) Discovery of high affinity inhibitors of *Leishmania donovani* N-myristoyltransferase. *MedChemComm* 6 (10), 1761−1766.

(17) Hutton, J. A., Goncalves, V., Brannigan, J. A., Paape, D., Wright, M. H., Waugh, T. M., Roberts, S. M., Bell, A. S., Wilkinson, A. J., Smith, D. F., Leatherbarrow, R. J., and Tate, E. W. (2014) Structure-based design of potent and selective *Leishmania* N-myristoyltransferase inhibitors. *J. Med. Chem.* 57 (20), 8664−8670.

(18) Bell, A. S., Mills, J. E., Williams, G. P., Brannigan, J. A., Wilkinson, A. J., Parkinson, T., Leatherbarrow, R. J., Tate, E. W., Holder, A. A., and Smith, D. F. (2012) Selective inhibitors of protozoan protein N-myristoyltransferases as starting points for tropical disease medicinal chemistry programs. *PLoS Neglected Trop. Dis.* 6 (4), e1625.

(19) Engstler, M., Thilo, L., Weise, F., Grunfelder, C. G., Schwarz, H., Boshart, M., and Overath, P. (2004) Kinetics of endocytosis and recycling of the GPI-anchored variant surface glycoprotein in *Trypanosoma brucei*. *J. Cell Sci.* 117 (7), 1105−1115.

(20) Overath, P., Stierhof, Y. D., and Wiese, M. (1997) Endocytosis and secretion in trypanosomatid parasites tumultuous traffic in a pocket. *Trends Cell Biol.* 7 (1), 27−33.

(21) Pereira, M. G., Nakayasu, E. S., Sant'Anna, C., De Cicco, N. N., Atella, G. C., De Souza, W., Almeida, I. C., and Cunha-e-Silva (2011) *Trypanosoma cruzi* epimastigotes are able to store and mobilize high amounts of cholesterol in reservosome lipid inclusions. *PLoS One* 6 (7), e22359.

(22) Wright, M. H., Paape, D., Storck, E. M., Serwa, R. A., Smith, D. F., and Tate, E. W. (2015) Global analysis of protein N-myristoylation

and exploration of *N*-myristoyltransferase as a drug target in the neglected human pathogen *Leishmania donovani*. *Chem. Biol.* 22 (3), 342−354.

(23) Brand, S., Norcross, N. R., Thompson, S., Harrison, J. R., Smith, V. C., Robinson, D. A., Torrie, L. S., McElroy, S. P., Hallyburton, I., Norval, S., Scullion, P., Stojanovski, L., Simeons, F. R., van Aalten, A. D., Frearson, J. A., Brenk, R., Fairlamb, A. H., Ferguson, M. A., Wyatt, P. G., Gilbert, I. H., and Read, K. D. (2014) Lead optimization of a pyrazole sulfonamide series of *Trypanosoma brucei* *N*-myristoyltransferase inhibitors: identification and evaluation of CNS penetrant compounds as potential treatments for stage 2 human African Trypanosomiasis. *J. Med. Chem.* 57 (23), 9855−9869.

(24) Brannigan, J. A., Roberts, S. M., Bell, A. S., Hutton, J. A., Hodgkinson, M. R., Tate, E. W., Leatherbarrow, R. J., Smith, D. F., and Wilkinson, A. J. (2014) Diverse modes of binding in structures of *Leishmania major N*-myristoyltransferase with selective inhibitors. *IUCrJ* 1 (Pt 4), 250−260.

(25) De Rycker, M., Hallyburton, I., Thomas, J., Campbell, L., Wyllie, S., Joshi, D., Cameron, S., Gilbert, I. H., Wyatt, P. G., Frearson, J. A., Fairlamb, A. H., and Gray, D. W. (2013) Comparison of a high-throughput high-content intracellular *Leishmania donovani* assay with an axenic amastigote assay. *Antimicrob. Agents Chemother.* 57 (7), 2913−2922.

(26) Jafari, R., Almqvist, H., Axelsson, H., Ignatushchenko, M., Lundback, T., Nordlund, P., and Molina, D. M. (2014) The cellular thermal shift assay for evaluating drug target interactions in cells. *Nat. Protoc.* 9 (9), 2100−2122.

(27) Paape, D., Bell, A. S., Heal, W. P., Hutton, J. A., Leatherbarrow, R. J., Tate, E. W., and Smith, D. F. (2014) Using a non-image-based medium-throughput assay for screening compounds targeting *N*-myristoylation in intracellular *Leishmania* Amastigotes. *PLoS Neglected Trop. Dis.* 8 (12), e3363.

(28) Walkinshaw, M. (2014) Multiple chemical scaffolds inhibit a promising *Leishmania* drug target. *IUCrJ* 1 (Pt4), 202−203.

(29) Panethymitaki, C., Bowyer, P. W., Price, H. P., Leatherbarrow, R. J., Brown, K. A., and Smith, D. F. (2006) Characterization and selective inhibition of myristoyl-CoA: protein *N*-myristoyltransferase from *Trypanosoma brucei* and *Leishmania major*. *Biochem. J.* 396, 277−285.

(30) Frearson, J. A., Wyatt, P. A., Gilbert, I. H., and Fairlamb, A. H. (2007) Target assessment for antiparasitic drug discovery. *Trends Parasitol.* 23 (12), 589−595.

(31) Wyatt, P. G., Gilbert, I. H., Read, K. D., and Fairlamb, A. H. (2011) Target validation: linking target and chemical properties to desired product profile. *Curr. Top. Med. Chem.* 11 (10), 1275−1283.

(32) Bochevarov, A. D., Harder, E., Hughes, T. F., Greenwood, J. R., Braden, D. A., Philipp, D. M., Rinaldo, D., Halls, M. D., Zhang, J., and Friesner, R. A. (2013) Jaguar: A high-performance quantum chemistry software program with strengths in life and materials sciences. *Int. J. Quantum Chem.* 113 (18), 2110−2142.

(33) Brand, S., Cleghorn, L. A. T., McElroy, S. P., Robinson, D. A., Smith, V. C., Hallyburton, I., Harrison, J. R., Norcross, N. R., Spinks, D., Bayliss, T., Norval, S., Stojanovski, L., Torrie, L. S., Frearson, J. A., Brenk, R., Fairlamb, A. H., Ferguson, M. A. J., Read, K. D., Wyatt, P. G., and Gilbert, I. H. (2012) Discovery of a novel class of orally active trypanocidal *N*-myristoyltransferase inhibitors. *J. Med. Chem.* 55 (1), 140−152.

(34) Copeland, R. A. (2005) *Evaluation of Enzyme Inhibitors in Drug Discovery: A Guide for Medicinal Chemists and Pharmacologists*, John Wiley & Sons, Hoboken.

(35) Goyard, S., Segawa, H., Gordon, J., Showalter, M., Duncan, R., Turco, S. J., and Beverley, S. M. (2003) An *in vitro* system for developmental and genetic studies of *Leishmania donovani* phosphoglycans. *Mol. Biochem. Parasitol.* 130 (1), 31−42.

(36) Nuhs, A., De Rycker, M., Manthri, S., Comer, E., Scherer, C. A., Schreiber, S. L., Ioset, J. R., and Gray, D. W. (2015) Development and validation of a novel *Leishmania donovani* screening cascade for high-throughput screening using a novel axenic assay with high predictivity

of leishmanicidal intracellular activity. *PLoS Neglected Trop. Dis.* 9 (9), e0004094.

(37) Wyllie, S., Patterson, S., Stojanovski, L., Simeons, F. R., Norval, S., Kime, R., Read, K. D., and Fairlamb, A. H. (2012) The anti-trypanosome drug fexinidazole shows potential for treating visceral leishmaniasis. *Sci. Transl. Med.* 4 (119), 119re1.

(38) Wyllie, S., and Fairlamb, A. H. (2006) Refinement of techniques for the propagation of *Leishmania donovani* in hamsters. *Acta Trop.* 97 (3), 364−369.

(39) Bradley, D. J., and Kirkley, J. (1977) Regulation of *Leishmania* populations within the host. I. the variable course of *Leishmania donovani* infections in mice. *Clin. Exp. Immunol.* 30 (1), 119−129.

(40) Kelly, J. M., Das, P., and Tomas, A. M. (1994) An approach to functional complementation by introduction of large DNA fragments into *Trypanosoma cruzi* and *Leishmania donovani* using a cosmid shuttle vector. *Mol. Biochem. Parasitol.* 65, 51−62.

(41) Hoyer, C., Mellenthin, K., Schilhabel, M., Platzer, M., and Clos, J. (2001) Use of genetic complementation to identify gene(s) which specify species-specific organ tropism of *Leishmania*. *Med. Microbiol. Immunol.* 190 (1−2), 43−46.

(42) Langmead, B., and Salzberg, S. L. (2012) Fast gapped-read alignment with Bowtie 2. *Nat. Methods* 9 (4), 357−359.

(43) Li, H., Handsaker, B., Wysoker, A., Fennell, T., Ruan, J., Homer, N., Marth, G., Abecasis, G., and Durbin, R. (2009) The Sequence Alignment/Map format and SAMtools. *Bioinformatics* 25 (16), 2078−2079.

(44) Glover, L., Alsford, S., Baker, N., Turner, D. J., Sanchez-Flores, A., Hutchinson, S., Hertz-Fowler, C., Berriman, M., and Horn, D. (2015) Genome-scale RNAi screens for high-throughput phenotyping in bloodstream-form African trypanosomes. *Nat. Protoc.* 10 (1), 106−133.

(45) Carver, T., Harris, S. R., Berriman, M., Parkhill, J., and McQuillan, J. A. (2012) Artemis: an integrated platform for visualization and analysis of high-throughput sequence-based experimental data. *Bioinformatics* 28 (4), 464−469.

(46) Ouakad, M., Bahi-Jaber, N., Chenik, M., Dellagi, K., and Louzir, H. (2007) Selection of endogenous reference genes for gene expression analysis in *Leishmania major* developmental stages. *Parasitol. Res.* 101 (2), 473−477.

(47) Franken, H., Mathieson, T., Childs, D., Sweetman, G. M., Werner, T., Togel, I., Doce, C., Gade, S., Bantscheff, M., Drewes, G., Reinhard, F. B., Huber, W., and Savitski, M. M. (2015) Thermal proteome profiling for unbiased identification of direct and indirect drug targets using multiplexed quantitative mass spectrometry. *Nat. Protoc.* 10 (10), 1567−1593.